Environmental Science
Water Research & Technology

ROYAL SOCIETY OF CHEMISTRY

TUTORIAL REVIEW

View Article Online
View Journal

Cite this: DOI: 10.1039/d0ew00679c

A review of phosphate adsorption on Mg-containing materials: kinetics, equilibrium, and mechanistic insights

Manoj Silva and Jonas Baltrusaitis *

Received 21st July 2020,
Accepted 24th September 2020

DOI: 10.1039/d0ew00679c

rsc.li/es-water

Significant efforts have been made to remove excess nutrient phosphorus in the form of aqueous phosphate ions from various wastewater streams to mitigate adverse environmental consequences to the watershed, such as eutrophication. Adsorption has long been a low-cost and highly effective method of phosphate removal which chiefly relied on immobilizing this valuable nutrient in low solubility solids. Magnesium-based adsorbents are emerging as an economically feasible solution to the phosphate removal problem that have the added benefit of facilitating nutrient recycling *via* the production of slow-release fertilizer. The current scientific literature on Mg-based adsorbents for phosphate has focused on a diverse range of techniques for the resulting material characterization, adsorption equilibrium and the observed kinetics making direct comparison between the diverse Mg-based adsorbents difficult. This tutorial review aims (a) to provide an overview of the state of the art in Mg-based phosphate adsorbents and (b) to propose a generalized data interpretation roadmap necessary to bridge the gap between the observed fundamental kinetics and mechanistic insights reported in the literature.

Water impact

Adsorption is a well-documented method of removing phosphate from wastewater in order to achieve low concentrations that would not lead to eutrophication. This review discusses the fundamentals (kinetics, mechanism, equilibrium, and characterization) of adsorption on Mg-based adsorbents, which are an emerging class of adsorbents that are low-cost and play a unique role in nutrient recycling.

Introduction

The advent of modern nitrogen (N) and phosphorus (P) fertilizer manufacturing has led to an unprecedented increase in food production capacity, which has sustained a rapid rise in population.[1,2] This rise in fertilizer demand has resulted in a complex N and P extraction, use, and end-of-life framework shown in Fig. 1 that is associated with significant energy consumption.[3,4] Furthermore, overuse of modern fertilizers has led to increased discharge of nutrients into the watershed from agricultural systems.[5] The discharge of even small concentrations of P can lead to eutrophication, which is known to restrict access to freshwater resources, harm aquatic ecosystems by forming dead spots, and cause significant greenhouse gas emissions.[5–11] Therefore, excess fertilizer application leading to loss of nutrients is unsustainable both economically and environmentally.

Phosphorus is mined from phosphate rock and is utilized unsustainably.[12,13] With the increasing trend of the global population, it is expected that the phosphorus consumption rate will increase. While the exact timeframe of reaching a peak in phosphorus demand is under debate, its occurrence poses significant challenges to food security and global geopolitics.[14] Therefore, capturing phosphate from wastewater and recycling is an important challenge to be addressed. While $MgCl_2$ has been used to produce a slow-release fertilizer struvite ($MgNH_4PO_4{\cdot}6H_2O$) from wastewater, the cost of soluble Mg precursors lower financial viability.[15] The use of low solubility Mg sources is an efficient and financially feasible process that proceeds *via* adsorption on a heterogeneous surface instead of homogeneous crystallization. Magnesium (Mg) is an alkaline-earth metal that is present as 2% of the earth's crust[16] and has a high affinity toward phosphate adsorption due to its smaller ionic radius (which leads to higher charge density).[17] Mg is also a

Department of Chemical and Biomolecular Engineering, Lehigh University, B336 Iacocca Hall, 111 Research Drive, Bethlehem, Pennsylvania 18015, USA. E-mail: job314@lehigh.edu; Tel: +1 610 758 6836

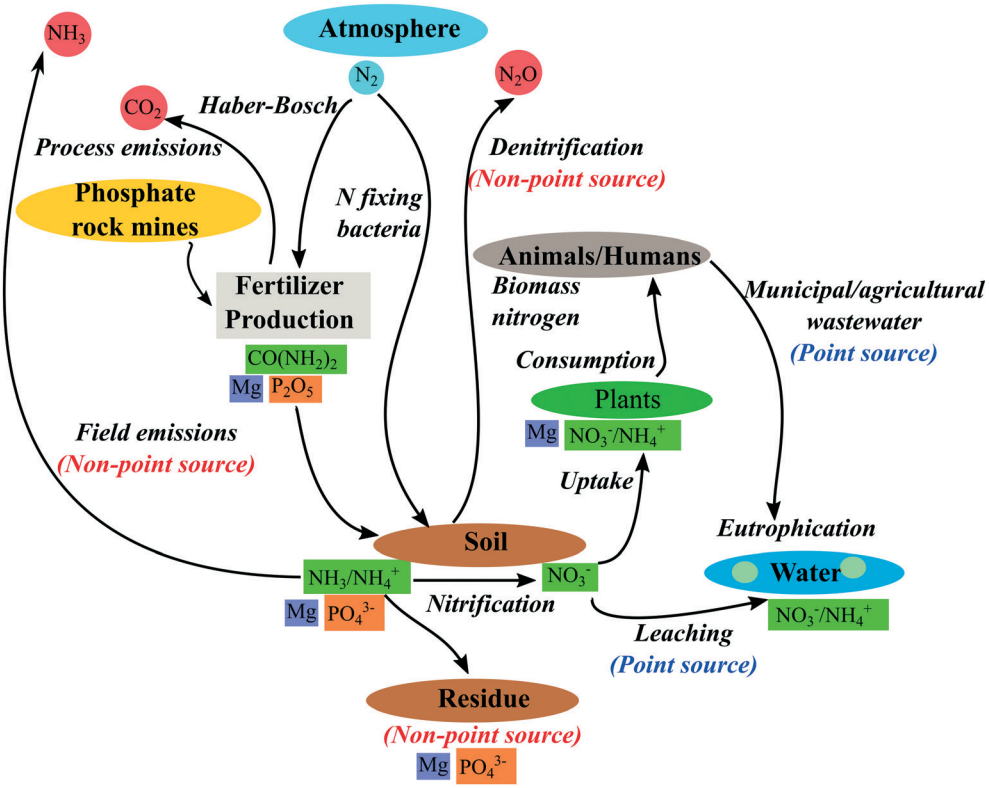

Fig. 1 The combined N and P cycles with an emphasis on non-point sources and point sources of nutrient loss.

critical macronutrient required for plant growth[18,19] and photosynthetic CO_2 fixation.[18,20,21] Since N, P, K fertilization has been considered to be more important in recent years, lack of Mg fertilization has led to acidic soils being more Mg deficient.[19,22] This Mg deficiency in soil has led to not only plant health issues, but also a reduction in Mg present in human diet leading to Mg deficiency in both developed and underdeveloped nations.[22] Phosphate adsorption using Mg-based sorbents allows for coupling the P-cycle with the Mg-deficiency problems and proposing unifying solutions to combat nutrient excess or shortage related problems.

Adsorption is a process where an adsorbate binds to a surface either *via* a physical bond (physisorption) or a chemical bond (chemisorption). Adsorbents are widely applicable for wastewater treatment, providing a convenient and low-cost method of pollutant removal.[23,24] A broad variety of material classes have been reported in the literature as potential phosphate adsorbents including but not limited to, bulk metal oxides,[25–27] supported metal oxides,[28–30] metal hydroxides,[31] and zeolites.[32,33] Adsorption kinetics, surface transformation mechanisms and reaction equilibria are inextricably interconnected and understanding the relationships that link them together is highly important in designing an efficient phosphate sorbent material. Previous reports have reviewed the broad material classes for phosphate adsorption,[34] discussed the fundamental interaction mechanisms of phosphate ions with the sorbents and the corresponding physicochemical parameters influencing phosphate–sorbent interaction strength,[17] and the economic aspects of using large-scale phosphate adsorption processes.[35] However, an important knowledge gap in the literature, as shown in this review, is the lack of insights in the surface compositional evolution as well as the adsorbed phosphate ion molecular structure transformation on the reactive Mg-containing solid sorbents. Consequentially, plenty of the reports have discussed observed (apparent) pseudo-order adsorption kinetics with the focus on the observed rate constants and equilibrium phosphate amounts removed from solution for different sorbents but rarely provided related mechanistic insights, such as surface structures of the adsorbed phosphate products or the transient intermediates.[27,36–39] Only recently have studies used *in situ* spectroscopy to understand phosphate adsorption related surface reactions on low solubility Mg-minerals, macroscopic particle level reconstruction, reactive intermediates and stable product speciation in an attempt to address this knowledge gap.[40] Present review focuses on analyzing molecular level details during phosphate ion adsorption since molecular level mechanistic understanding can further provide context for the pseudo kinetic model fits found in the literature and, ultimately, guide the design of novel materials for wastewater treatment.

In particular, this review aims to provide a clear overview of the current progress using Mg-based materials for phosphate adsorption/structural transformation. Specifically,

this review will discuss the current Mg-based adsorbent material types and methods of their characterization with emphasis on the surface properties, various kinetic models used to analyze phosphate ion adsorption performance, quantitative equilibrium analysis *via* isotherms and relevant thermodynamic parameters, as well as the adsorption mechanisms and how kinetics are related to the low solubility Mg-containing mineral surface transformations.

Magnesium-based adsorbents in wastewater treatment and characterization

Mg-based adsorbents have been reported in a variety of forms and thus, we can classify them as supported (the Mg compound is deposited on the surface of support material) and unsupported (the Mg compound is in bulk form) adsorbents as shown in Fig. 2.

Tuning the surface species and the pore textural properties allows for increasing the performance of the adsorbent by changing adsorption kinetics.[41] Ultimately, the synthesis of a high surface area and highly porous adsorbent is desired for better performance.[42] Utilizing a high surface area support helps achieve high dispersion of Mg sites, while the increased porosity of support can yield better transport properties compared to bulk materials with less porosity. Supports such as diatomite and bentonite exhibit very low phosphate adsorption when utilized in the raw form, while ZrO_2 exhibits significant phosphate adsorption.[38,39,43,44] A support material with high stability and minimal dissolution is desired for phosphate adsorption. While supported materials provide high dispersion, in the case of phosphate recovery (*e.g.* as struvite) it may be less favorable since the final product may contain the support material which reduces the purity. In the case of unsupported materials, synthetic adsorbents afford higher tunability in terms of shape, surface area, and pore structure, but require additional chemicals and processing steps. The use of natural minerals can circumvent the need for complicated material synthesis but may include contaminants such as heavy metals.[45] However, natural minerals can be a more sustainable Mg source for struvite recovery due to the abundance and low cost.[15]

Supported Mg-based adsorbents are typically synthesized *via* hydrothermal synthesis[46] and sol–gel synthesis.[27] In the case of the hydrothermal synthesis, the authors utilized a combination of hydrothermal treatment with redispersion in deionized water and calcination to produce high surface area MgO. The re-dispersion resulted in doubling the surface area over the sample that was not re-dispersed, which increased the phosphate adsorption capacity from 165.29 mg g^{-1} to 255.1 mg g^{-1}.[46] A study using spherical MgO nanoparticles for phosphate adsorption demonstrated the use of a structure-directing agent sodium poly(4-styrenesulfonate) to achieve spherical morphology. Typically supported Mg-based adsorbents were prepared *via* precipitation of $Mg(OH)_2$ in the case of diatomite[30,39,47] and bentonite,[48,49] and biochar[44] which in some cases was followed by calcination to produce MgO. In a report by Lin *et al.*, $Mg(OH)_2/ZrO_2$ adsorbent was prepared *via* co-precipitation resulting in a significantly high surface area of 195 m^2 g^{-1}. However, without the use of a structure-directing agent, controlling morphology in precipitation methods can be difficult. These facile methods primarily require materials of low hazard levels in handling and deliver reproducible results.

Material characterization of adsorbents can be done to elucidate information regarding the bulk crystal structure, surface characteristics, molecular and electronic structure, and pore structure. Fig. 3 shows some of the prevalent techniques in characterizing phosphate adsorbents.

Bulk characterization techniques are important in identifying the material species present in the adsorbent and their bulk crystalline or amorphous phase(s). Powder X-ray diffraction (pXRD) is one of the most common techniques utilized to identify crystalline phases in a solid powder material. Multiple Mg-based adsorbent reports have utilized pXRD to characterize the bulk structure of the adsorbent.[15,39,40,46,48–51] In the case of naturally derived[40] or process-byproduct magnesium material[52,53] sources, pXRD allows for a good starting point in material characterization by crystalline phase identification. pXRD also allows for crystallite size quantification by applying the Debye–Scherrer equation to the peak widening.[54] One of the advantages of pXRD is that it analyzes an average of all grains present in the powder sample and thus, it does not provide local information as done by microscopy. However, pXRD does not provide any surface-specific information and thus, may not

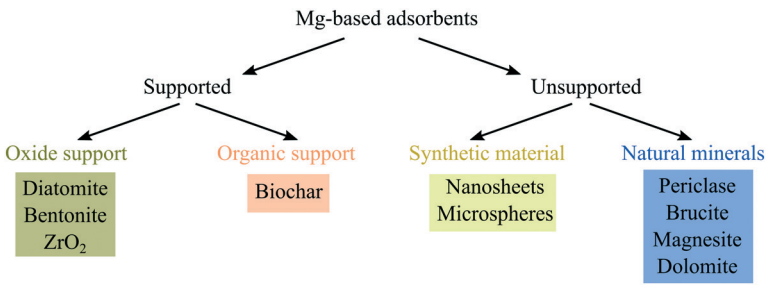

Fig. 2 Different types of Mg-based adsorbents.

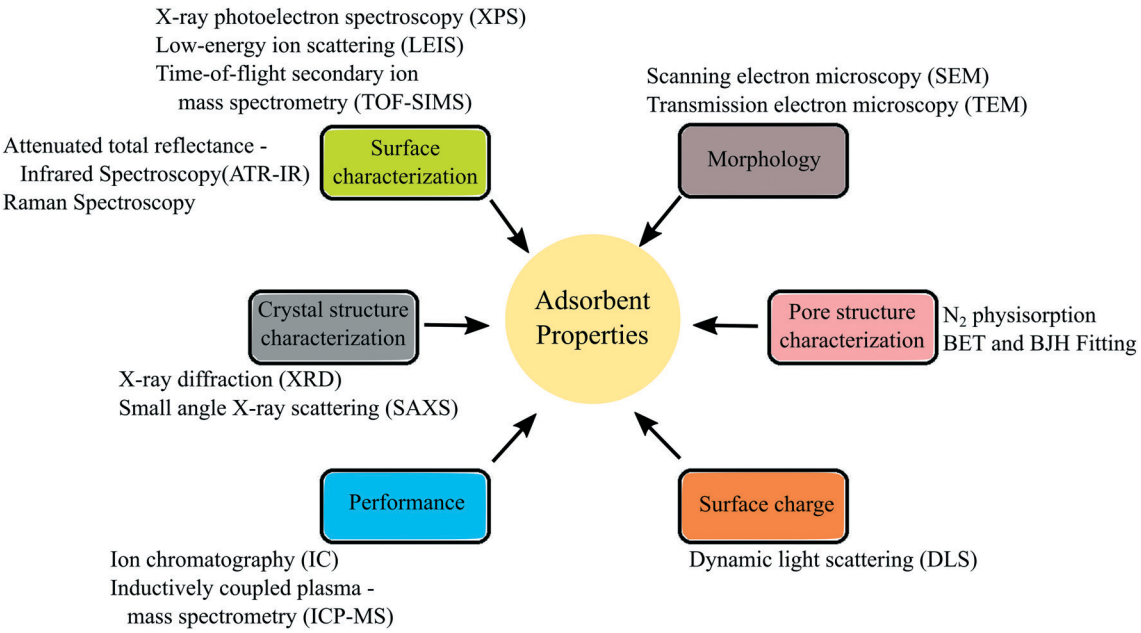

Fig. 3 Material characterization techniques related to adsorbents.

provide insights regarding adsorption characteristics of a surface. Further bulk information such as particle size and morphology can be studied using electron microscopy techniques, namely, scanning electron microscopy (SEM) and transmission electron microscopy (TEM). Energy-dispersive X-ray spectroscopy (EDS) is typically coupled with electron microscopy analysis and produces elemental analysis spectra. EDS typically detects bulk components over 0.1 wt% and other major components but is not suitable for trace element detection (under 0.1 wt%).[55,56] X-ray absorption spectroscopy (XAS) and ^{31}P nuclear magnetic resonance spectroscopy (NMR) are two techniques that characterize the bulk material and can provide important coordination information for P in the adsorbed product.[57–59]

Pore structure characterization becomes important in identifying the pore texture information, which holds implications for the diffusion properties of the adsorbent. Nitrogen physisorption data analyzed using the Brunauer–Emmett–Teller theory and Barrett–Joyner–Halenda theory can quantify surface area and pore structural information respectively.[60,61] Table 1 shows the surface area and pore volume information reported for Mg-based phosphate adsorbents. As a bulk material MgO has been reported to have a low surface area and porosity[15] but by using a support such as biochar[62] or diatomite[39,47] to achieve higher dispersion of MgO sites and porosity, it has been reported that it is possible to attain higher reaction rates. Furthermore, in the case of MgO, it has been proven that by fabricating mesoporous MgO structures it is possible to increase surface area and pore volume.[27,39,62,127] The pore characteristics of the adsorbent dictate the transport of phosphate through the material which in turn affects the rate of adsorption. To increase the rate of adsorption, increasing the pore volume and surface area is of interest *via* the use of support material or mesoporous particle fabrication as discussed above. However, it is important to note that BET and BJH information is gained on dry powder, while the adsorbent may behave differently in the aqueous environment due to dissolution and potential pore collapse. Analysis before and after application in aqueous environment can provide some insight on whether significant area loss and pore blocking due to phosphate has occurred.

Surface characterization of adsorbent materials should be done carefully since the surface sensitivity of different techniques can vary significantly. High sensitivity low-energy ion scattering (HS-LEIS) can be utilized to probe the first several monolayers of a material and measure elemental composition with capability for static depth profiling.[63–65] However, in the case of adsorbents used in the aqueous phase, the surface undergoes dissolution and restructuring and thus, an understanding of the transformations of the surface region becomes important. For the characterization of this surface region of the complex reconstructed surfaces, X-ray photoelectron spectroscopy (XPS) and time-of-flight secondary ion mass spectroscopy (ToF-SIMS) are well-suited. XPS is a widely used adsorbent characterization to obtain chemical state information in the surface region. Notably, these are vacuum techniques that will perform *ex situ* analysis so the role of hydration on surface structures must be considered carefully. The use of diffuse reflectance infrared Fourier transform spectroscopy (DRIFTS) and Raman spectroscopy are two other spectroscopies used to report surface information.[39,66] However, given the penetration depths of the lasers used in both spectroscopies it is important to note that both DRIFTS and Raman spectroscopy yield bulk and surface information unless the overlayer is

Table 1 Operating conditions for Mg-based phosphate adsorbent studies and characterization

Adsorbent	Wastewater source and initial phosphate concentration (ppm)	Adsorbent loading (ppm)	Experimental conditions	Adsorption capacity (mg PO_4/g)	BET surface area (m^2 g^{-1})	Pore volume (cm^3 g^{-1})
MgO/diatomite[39]	120	300	25 °C, initial pH = 7.0	168.07 (PSO)	34.78	0.195
MgO/diatomite[47]	62	500	25 °C, initial pH = 7.0	121.7 (PSO)	35.76	0.213
$Mg(OH)_2$ and bentonite composite/biochar[49]	60	400	25 °C, initial pH = 7.0	125.36 (PSO)	68.66	0.32
$Mg(OH)_2$/bentonite[73]	40	2000	45 ± 0.1 °C, initial pH 6.0 and 7.0	741.14[a] (EXP)	51.72	Not reported
MgO microspheres[27]	10	200	30 °C, pH = 5.0	13.51(PSO)	72.10	0.31
$Mg(OH)_2/ZrO_2$ (ref. 43)	20	600	25 °C, pH = 7.0	32.5 (PSO)	195.9	0.1604
$Mg(OH)_2$/diatomite[30]	50	500	25 °C, pH = 5.0	45.7 (PSO)	72.53	0.26
MgO–biochar nanocomposite[44]	20	100	22 °C	835 (L)	70.0	Not reported
CaO–MgO–C composite[36]	857	1250	Initial pH = 5.83	621 (L), 19.98 g mg^{-1} (PSO)	169.33	0.150
MgO/magnetic biochar[38]	50	2500	23 °C, pH = 4.0	121.25 (L)	27.22	0.343
$MgFe_2O_4$/biochar[37]	100, 200, 300	200	20 °C, pH = 3.0	163.91, 219.76, 290.79 (PSO)	172.81	0.247
4 : 1 Mg/Al-LDHs biochar[74]	50	2500	23 °C, pH = 3.0	81.83 (L) 20.07 (PSO)	12.25	0.016
MgO nanosheets[46]	50	400	23 °C, pH = 5.0	255.1 (PSO)	30.13	0.17
MgO (ref. 15)	500	300	25 °C, initial pH = 5.4	833 (PSO)	94	Not reported
$MgCO_3$ (ref. 50)	500	1000	25 °C, initial pH = 5.4	—	—	Not reported
Calcined $CaMg(CO_3)_2$ (ref. 40)	500	500	25 °C, initial pH = 5.4	909 (PSO)	—	Not reported
MgO/biochar[75]	5–200	1000	20 °C	579.9 (L)	56.4	Not reported
Amorphous $MgCa(CO)_3$	0–2340	5000	25 °C, pH = 10.0		55.93	Not reported

[a] Values calculated using the reported adsorption capacity (mg m^{-2}) and surface area (m^2 g^{-1}). L, Langmuir. PSO, pseudo-second order.

probed carefully.[67] Raman spectroscopy is a powerful tool to study adsorption processes *in situ*, given the ability to utilize liquid phase cells and the lack of interference by water observed in infrared spectroscopy.[40,68] ATR-IR (attenuated total reflectance) has also been utilized successfully to study the interface of aqueous adsorption reactions *via* the use of flow cells.[69–71] The sensitivity of ATR-IR spectroscopy toward the protonation of the phosphate group allows for clear discrimination of surface phosphate species using the nondegenerate symmetric stretching ν_1, and the triply degenerate symmetric stretching ν_3. The tetrahedral symmetry of $PO_{4(aq)}^{3-}$ (T_d point group) has one active ν_3 band, while in $HPO_{4(aq)}^{2-}$ the symmetry reduces from T_d to C_{3v} leading to the ν_3 band split (to two bands) and ν_1 band activation. Finally, in the case of $H_2PO_{4(aq)}^{-}$, the symmetry is reduced to C_{2v} and the ν_3 band is split into three bands and ν_1 remains active.[71] Elzinga and Sparks have discussed in detail the surface species formed on hematite over a wide range of pH conditions using ATR-IR.[71] Similar work on substrates such as brucite and magnesite would be invaluable in understanding the surface speciation of phosphate complexes. Kiani *et al.* have demonstrated using *in situ* Raman spectroscopy that the calcined dolomite surface undergoes a complex surface transformation during phosphate adsorption.[40] The starting calcined dolomite surface contains –OH groups that serve as adsorption sites for dissolved CO_2, forming $-CO_3^{2-}$ groups (evidenced by the 1086 cm^{-1} band). These $-CO_3^{2-}$ groups are replaced by low-symmetry polymeric $H_2PO_4^{-}$ chains.[40] Time-resolved Raman and ATR-IR spectroscopies are key tools in observing these surface transformations, providing insights that can lead to rational design of novel adsorbent materials.

The surface charge characterization is important in determining the strength of Coulombic interactions between the phosphate ions and the adsorbent, while the surface composition and molecular structures are important in determining the adsorption mechanism. Functional groups on the adsorbent surface such as –OH, $-HCO_3^{-}$ and $-CO_3^{2-}$ groups on MgO may influence the surface charge by producing charge deficits. Zeta potential is typically used to quantify the surface charge of a particle suspended in an aqueous phase and is dependent on the solution pH and ionic strength. A previous study on using MgO for phenol ozonation has reported the zeta potential of the MgO particle surface as a function of pH.[72] In this study Wang *et al.* show that MgO is positively charged beyond pH = 9, which is the region of interest for phosphate adsorption and struvite formation.[72] In the case of MgO–diatomite,[47] the authors note that MgO–diatomite is positively charged in the pH range of 2.0 to 10.0, with the isoelectric point at pH = 11.

This shows that phosphate adsorption can occur over a wide range of pH values.

Adsorption kinetics of aqueous phosphate on the adsorbent surface

Kinetics of adsorption are typically depicted by constructing plots of the adsorbed quantity as a function of time. The shape of the plot indicates the nature of the adsorption process and how to model the kinetics. In typical phosphate adsorption studies, batch experiments are used to collect data with experimental parameters such as pH, temperature, adsorbent loading, initial phosphate concentration varied. The phosphate adsorbed at time t per mass of adsorbent m is shown by eqn (1).

$$q_t = \frac{(C_0 - C_t)V}{m} \quad (1)$$

where the initial concentration of phosphate in the solution phase is denoted by C_0 (mg L^{-1}) and the concentration in the solution phase at time t (min) is denoted by C_t (mg L^{-1}). The volume of the batch is denoted by V (L). Batch experiments are commonly utilized since intrinsic kinetics can be studied. Intrinsic kinetics are the kinetics of adsorption in the absence of mass transfer limitations. Higher agitation speeds lead to smaller boundary layers which eliminate film diffusion limitations. Using smaller particle sizes for the adsorbent can minimize intraparticle diffusion limitations.

Reaction-controlled kinetics

Adsorption occurs when an adsorbate molecule diffuses to the surface of the adsorbent and undergoes either physisorption or chemisorption as discussed above and shown in Fig. 4. If a process has rapid diffusion to the surface and the bond formation is the slower step, the process is referred to as a reaction-controlled process. In this case, the rate of diffusion preceding the reaction is considered negligible. Phosphate adsorption kinetics have been analyzed by pseudo-first order, pseudo-second order, and Elovich kinetics as shown in Fig. 4.

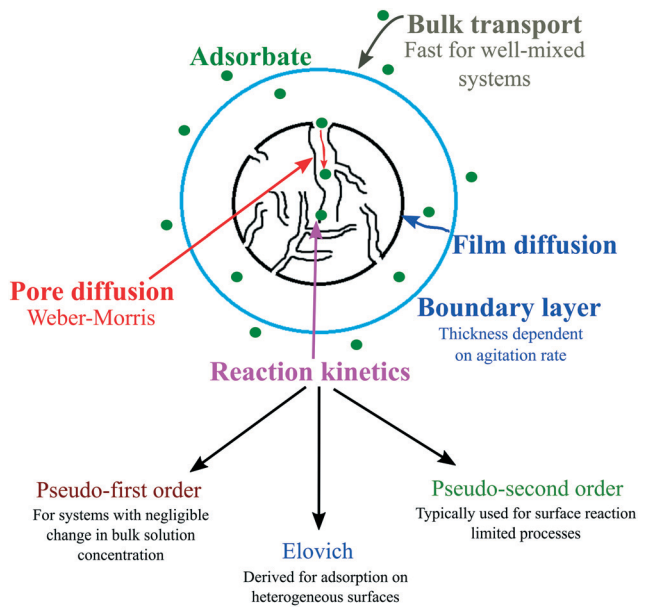

Fig. 4 The diffusion and surface reaction processes occurring on the porous adsorbent particle during adsorption.

The pseudo-first order equation shown by eqn (2) was proposed in 1898 by Lagergren[76] and is still widely applied for characterizing adsorption processes.[50]

$$\frac{dq_t}{dt} = k_1(q_e - q_t) \quad (2)$$

In this equation q_t (mg g^{-1}) and q_e (mg g^{-1}) denote the adsorbed species concentration at time t (min) and equilibrium, respectively. k_1 (mg g^{-1} min^{-1}) denotes the pseudo-first order reaction constant. By integrating this equation using the boundary conditions time $t = 0$ and $t = t$, as well as $q_t(t = 0) = 0$ and $q_t(t = t) = q_t$ the following form can be used as shown by eqn (3).

$$\log(q_e - q_t) = \log(q_e) - \frac{k_1}{2.303}t \quad (3)$$

Ho and McKay have discussed two important aspects of this equation: (1) the $k_1(q_e - q_t)$ parameter does not represent the number of available adsorption sites. (2) The intercept $\log(q_e)$ term does not necessarily equate the log value of the concentration of adsorbed material at equilibrium.[77] When fitting experimental data to eqn (3) the q_e value must be known in advance. However, since achieving equilibrium requires lengthy periods in adsorption experiments, this value is typically approximated. Therefore, goodness-of-fit parameters may not be high for pseudo-first order fitted data. Most Mg-based adsorbents do not fall under the pseudo-first order kinetics but, $MgCO_3$ (ref. 50) and MgO-byproduct[52] utilization for struvite crystallization have been discussed as pseudo-first order processes. However, in the case of MgO-byproduct, the authors do not provide the R^2 values for their fits and do not discuss attempting pseudo-first *vs.* pseudo-second order to discriminate which model fits better. Furthermore, this report shows that 67.67% of the adsorbent was MgO which shows pseudo-second order kinetics but does not discuss any reasoning for the observation of pseudo-first order. Therefore, only the $MgCO_3$ report is considered to be an example of the pseudo-first order equation being used to model phosphate adsorption in this review (the validity of this fit will be debated later in the review).

When using the use of pseudo-order models, researchers must consider the physical significance of these models in their systems, rather than only considering the mathematical significance (*i.e.* considering only R^2 values). The pseudo-first order model has been discussed extensively by Azizian in his work on activated adsorption/desorption derivation[78] as well as Rudzinski and Plazinski in their work on statistical rate theory derivation[79] to reconcile the physical meaning

corresponding to adsorption kinetics and the "lumped" mathematical parameters in the equation. Rudzinski and Plazinski have discussed that the pseudo-first order model can be derived for both intraparticle diffusion-controlled processes and surface reaction controlled processes but, the physical meaning of the rate constants varies in the two scenarios.[80] Azizian's report states that the pseudo-first order model only holds in scenarios where the change in the bulk solution concentration of the adsorbate is negligible.[78] Focusing on the one case of the $MgCO_3$, it is clear that applying the pseudo-first order equation to the entire 120 minute reaction time is unrealistic given the bulk concentration changes by over 85% during this time.[50] This condition would generally prohibit the use of pseudo-first order models in the case of phosphate adsorption since a high-performance adsorbent is generally desired to have high removal in a short period, which does not align with the abovementioned assumption of negligible change in bulk concentration. The high R^2 fit reported[50] is possibly a mathematical artifact, devoid of physical significance. McKay *et al.* have discussed that the adsorption data should not be fitted beyond the first 20–30 minutes of reaction and that the errors of q_e from pseudo-first order can potentially be from some initial boundary layer transport resistance.[81]

The pseudo-second order model has been widely applicable in phosphate adsorption data for Mg-based adsorbents.[15,27,39,40,48,51] eqn (4) as proposed by Blanchard *et al.*[82] shows the rate equation for the pseudo-second order.

$$\frac{dq_t}{dt} = k_2(q_e - q_t)^2 \quad (4)$$

Here k_2 (g mg^{-1} min^{-1}) denotes the pseudo-second order apparent rate constant. Similar to the previous pseudo-first order equation, this can also be solved with appropriate boundary conditions to present a linear form that is more suitable for fitting data as shown by eqn (5).

$$\frac{t}{q_t} = \frac{1}{q_e}t + \frac{1}{k_2 q_e^2} \quad (5)$$

Many authors have reviewed the use of the pseudo-second order equation extensively in the context of pharmaceutical, polymer, and heavy metal removal from wastewater.[77,83–86] However, a limited number of reviews have been published on the kinetic analysis of phosphate adsorption.[17] Unlike pseudo-first order kinetics, the pseudo-second order kinetics do not assume the q_e value but calculate it using the slope of the fit. This, in turn, is used to calculate k_2 from the intercept. Table 2 shows a summary of relevant kinetic equations discussed in this review and how the data is plotted to calculate adsorption parameters. The physical insight typically gained from the pseudo-second order fitting is that the adsorption is surface-reaction limited.[15,39,40] This has been compared to *in situ* spectroscopic experimental evidence of this surface-reaction in one study (discussed later on).[40] Materials based on MgO have been shown to consistently follow pseudo-second order kinetics[15,39,43,47] in both bulk and supported form, as well as the materials that contain CaO (ref. 36 and 40) indicating that the rate-limiting surface reaction step would be similar across all materials. It is important to note that Azizian has reported the k_2 value to be an apparent rate constant, which is a complex function of the initial concentration of adsorbate in solution.[78] There is an intimate relationship between the reaction mechanism and the apparent kinetics of a process, and understanding this is imperative to properly model the kinetics of a system. The adsorption mechanism section below contains further discussion on the physical significance of different kinetics models. The kinetic parameters reported using these pseudo-order models act more as data-fitting exercises and most do not provide insight on process design and scale-up.

The Elovich equation[87] proposed by Roginsky and Zeldovich has been applied in some cases to model the kinetics of phosphate adsorption.[47,49] Elovich equation (eqn (6)) is aimed to model adsorption that follows Langmuir kinetics but accounts for the surface heterogeneity.

$$\frac{dq_t}{dt} = \alpha e^{-\beta q_t} \quad (6)$$

Here α denotes the initial reaction rate and β denotes an experimental constant. Parravano and Boudart have discussed the Elovich equation as a generalized equation that discussed diffusion and surface reaction processes in combination and thus, unable to provide information about an exact mechanism.[88] The linear form of the Elovich equation is as given below by eqn (7).

$$q_t = \frac{1}{\beta}\ln(\alpha\beta) + \frac{1}{\beta}\ln(t) \quad (7)$$

In reports by Jing *et al.*[49] and Li *et al.*,[47] the Elovich equation produced fits that had lower R^2 values than the pseudo-second order. While the Elovich equation is expected to be

Table 2 Relevant kinetic models of adsorption and plots to fit experimental data

Equation	Linear form	Plot	Relevant parameters
Pseudo-first order	$\log(q_e - q_t) = \log(q_e) - \frac{k_1}{2.303}t$	$\log(q_e - q_t)$ *vs.* t	k_1 = slope × 2.303
Pseudo-second order	$\frac{t}{q_t} = \frac{1}{q_e}t + \frac{1}{k_2 q_e^2}$	t/q_t *vs.* t	q_e = 1/slope k_2 = (slope)^2/intercept
Elovich	$q_t = \frac{1}{\beta}\ln(\alpha\beta) + \frac{1}{\beta}\ln(t)$	q_t *vs.* $\ln(t)$	β = 1/slope α = (slope)exp(intercept/slope)
Weber and Morris	$q_t = k_p\sqrt{t} + C$	q_t *vs.* $t^{1/2}$	k_p = slope C = intercept

applied toward a variety of systems where activated adsorption is occurring, the low presence of its application in the phosphate adsorption literature may be due to its weakness in factoring in surface reconstruction.[89] Since $\ln(t) \rightarrow \infty$ as $t \rightarrow \infty$, q_t is predicted to be an infinite value over a long period which is physically unrealistic. Given that most kinetic experiments for phosphate adsorption are conducted in batch mode the equilibrium adsorbed concentration (q_e) is expected to be a finite value. This is a major weakness of the Elovich equation and therefore, is not widely used to describe overall kinetics of adsorption.

To compare the adsorption kinetics for various Mg-based adsorbents, we suggest normalizing by the reported surface area values. These surface area normalized values provide a more realistic comparison for apparent k_2 values since the adsorbent compounds can be bulk, supported, as well as nanostructured materials with varying surface areas, which has a significant impact on adsorption. Fig. 5 shows the surface area normalized apparent k_2 values for select adsorbents that have reported BET surface area and optimal loading. Eqn (8) was used to calculate the phosphate removal (kg per day).

$$\left[\text{Phosphate removal}\left(\frac{\text{kg}}{\text{day}}\right)\right] = \left[\text{Rate constant}\left(\frac{\text{kg PO}_4}{\text{mg adsorbent}^{-1}\ \text{min}^{-1}}\right)\right] \times \left[\text{Adsorbent loading}\left(\frac{\text{mg}}{\text{L}}\right)\right] \times [\text{Contact time (min)}] \times \left[\text{Wastewater flow rate}\left(\frac{\text{L}}{\text{day}}\right)\right] \quad (8)$$

The calculations were done for adsorbents that for pseudo-second order kinetics for ease of comparison. In each case, the optimal loading reported at 298 K was used. The contact time of 2 hours was used along with the 4.4 billion liters of wastewater produced per day which corresponds to the value for Beijing published in IWA Wastewater Report 2018.[90] The lower bound for phosphate recovery per day was calculated using the data for the $Mg(OH)_2$ and bentonite composite supported on biochar,[49] which has the lowest normalized apparent k_2. The upper phosphate removal limit was calculated using the performance reported by Li *et al.* with the 4 : 1 Mg–Al layered double hydroxide supported on biochar.[74] The supported adsorbents and the bulk adsorbents show comparable k_2 values. The MgO–CaO–C, MgO/diatomite, and MgO microspheres show similar surface area normalized k_2 values which shows that while the more efficient transport in the supported materials allows for faster adsorption, the low number of Mg-sites can be a weakness. The MgO microspheres have improved transport compared to bulk MgO and have more Mg-sites which leads to similar performance as the MgO/diatomite and MgO–CaO–C. Therefore, tuning loading and the intraparticle transport properties to optimize the adsorption rate becomes an important consideration during material design.

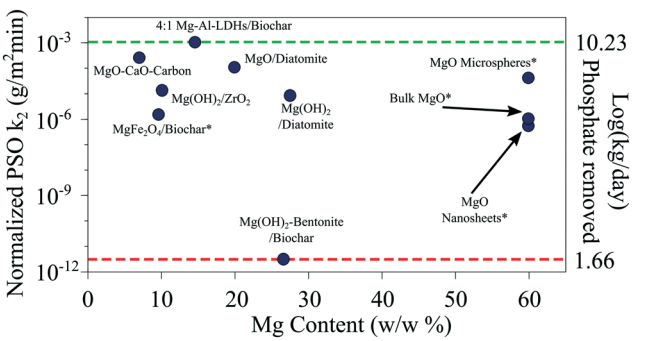

Fig. 5 Normalized apparent pseudo-second order (PSO) adsorption rate constant k_2 normalized by reported BET surface area for Mg-based phosphate adsorbents (*denotes Mg content not reported. These values were calculated using the synthesis reported in the experimental method). The green line denotes maximum phosphate removal per day and the red line denotes the minimum phosphate removal per day calculated by eqn (8).

Diffusion-controlled kinetics

The transport of phosphate during the adsorption can be viewed in three separate regimes: 1) phosphate diffusion in the bulk solution 2) phosphate diffusion to the surface of the adsorbent from the bulk solution through the hydrodynamic boundary layer 3) diffusion within the pores of the adsorbent. The diffusion in the bulk solution is typically nearly instantaneous for well-mixed systems and thus, cannot realistically be the limiting step for an adsorption process. The rate of adsorption when phosphate diffusion from the bulk solution through the boundary layer (film diffusion) is the limiting step can be described using the linear form of the film diffusion shown by eqn (9) as described by Tien.[91]

$$\frac{dq}{dt} = J_f = k_f(C_{bulk} - C_{surface}) \quad (9)$$

In eqn (9) the flux of phosphate is denoted by J_f, the diffusion coefficient is k_f, the bulk and adsorbent surface concentrations are denoted by C_{bulk} and $C_{surface}$. The driving force for the diffusion is the concentration difference between the bulk and surface, *i.e.* over the boundary layer (film). In a well-mixed batch reactor, the film diffusion is typically not rate-limiting. Therefore, in a case such as struvite crystallization in which a semi-continuous batch reactor is favored over an adsorption column the film diffusion step does not become rate-limiting. The final case of transport in adsorption is pore diffusion or intraparticle diffusion, assuming that diffusion through the pore fluid is the only contribution. For a single species, Fick's law is applied and the macroscopic conservation equation is as shown by eqn (10).

$$\varepsilon_p \frac{\partial C}{\partial t} + \rho_p \frac{\partial q}{\partial t} = \frac{1}{r^2}\frac{\partial}{\partial r}\left(D_p r^2 \frac{\partial C}{\partial r}\right) \quad (10)$$

In eqn (10), C and q refer to the adsorbate concentration in the bulk liquid and adsorbed on the surface respectively, ρ_p denotes the particle density, r denotes particle radius (assuming spherical particle), ε_p denotes the adsorbent particle porosity, and D_p denotes the pore diffusivity. In the phosphate adsorption literature, the experimentally derived Weber and Morris equation[92] has also been utilized across a describes the process as shown by eqn (11).

$$q_t = k_p\sqrt{t} + C \quad (11)$$

In the Weber and Morris equation q_t denotes adsorbed concentration, k_p denotes the intraparticle diffusion coefficient, t denotes time, and C is a fitting coefficient of which the magnitude describes the involvement of intraparticle diffusion in the rate-limiting step. In a scenario where the data fits a line through the origin, intraparticle diffusion is the rate-limiting step. Jing *et al.* have reported intraparticle diffusion analysis of $Mg(OH)_2$/bentonite composite supported on biochar showing that there is a multi-regime adsorption behavior.[49] In the time range from 4–6 minutes, the k_p value is reported as 17.37 mg g^{-1} $min^{-0.5}$ and in the time range of 7–13 minutes, the k_p value is reported as 4.86 mg g^{-1} $min^{-0.5}$. Similar behavior is reported for $MgFe_2O_4$ showing multi-regime phosphate adsorption transport.[37] This shows that the intraparticle diffusion is rapid at the beginning of the process, but later on the rate decreases possibly due to pore blocking or active-site depletion. Pore textural property characterization is important for fully understanding the transport properties of an adsorbent and designing new adsorbents should be done with increased porosity in mind due to the advantage of faster pore diffusion.

Adsorption mechanisms of phosphate on Mg-sorbent surfaces

Phosphate adsorption on metal oxide-based adsorbents is known to primarily occur *via* the inner-sphere complexation mechanism.[17,93,94] A recent review has thoroughly reviewed the different mechanisms of phosphate adsorption on a variety of adsorbent materials not limited to metal oxide-based adsorbents.[17] Therefore, this review aims to discuss the relationship between kinetic models and the mechanism of adsorption, rather than to restate what the previous review has discussed.

The adsorbents considered in this review are primarily MgO, $Mg(OH)_2$, or $MgCO_3$ materials. Once added to the solution phased containing the phosphate ions, the surface of the adsorbent is expected to undergo hydration and dissolve. For the 600 ppm monoammonium phosphate solution used in several studies, the initial pH is ~5.4 at which the rate-controlling step of MgO surface dissolution is the diffusion-limited proton transfer from the solution to the surface.[95] However, with increasing pH the reaction of MgO with water is expected to produce $Mg(OH)^+$ species on the surface as reported by Stolzenburg *et al.*[26] Following its formation, the $Mg(OH)^+$ species releases Mg^{2+} and $2OH^-$. The release of Mg^{2+} ions is expected to form a thin supersaturated boundary layer over the surface. This phenomenon has been recorded previously on other mineral interfaces as well, leading to nucleation of insoluble crystalline products within the boundary layer or at the surface.[96–98] Hövelmann and Putnis have discussed the surface transformation *via* the use of atomic force microscopy (AFM) during the nucleation and growth of struvite crystals on the brucite surface.[98] The authors discuss the importance of the surface dissolution for the low-solubility brucite material. The bulk solution concentration of Mg^{2+} is relatively low and is not sufficient for the removal of phosphate since the supersaturation limit is not met. However, at defect sites such as steps where undersaturated atoms are present, struvite nucleation is facilitated. This may be due to the higher propensity of the undersaturated sites to undergo dissolution and form supersaturated Mg^{2+} solution layers over the particle leading to seed crystal nucleation. Thus, whether the process should be considered phosphate adsorption (on the surface) or crystallization (in the boundary layer near the surface) is of importance for the clarity of future work.

Understanding the surface dissolution and restructuring steps becomes highly important in understanding the validity of kinetic model results. Kinetic equations are mathematical expressions and while high R^2 values can be obtained from a model, it does not necessarily provide correct physical insights into the adsorption process. The opposite must be considered. One must acquire the physical insights *via in situ* characterization and then

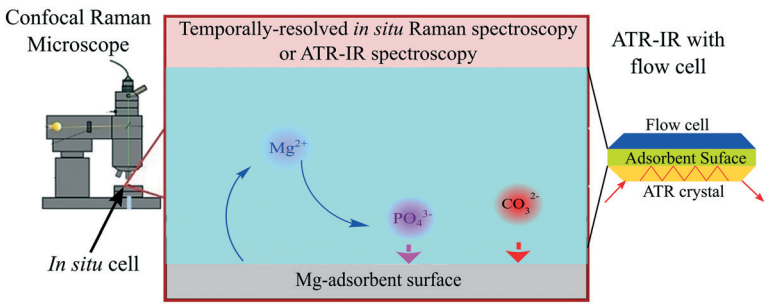

Fig. 6 The use of *in situ* Raman spectroscopy and ATR-IR spectroscopy to monitor surface transformations during phosphate adsorption.

consider which model to apply to report useful and accurate information in the literature. For the case of phosphate adsorption on Mg-based adsorbents, two cases should be considered: (i) the case of precipitating phosphate as a magnesium phosphate with no ammonium ions present in solution, and (ii) the precipitation of phosphate as struvite in the presence of ammonium. In the case of struvite formation, often the kinetics are reported as pseudo-second order for MgO-based adsorbents[15,39] and in one case as mentioned above, pseudo-first order for $MgCO_3$.

Vibrational spectroscopy techniques such as IR and Raman spectroscopies can provide important mechanistic information about phosphate adsorption on mineral interfaces (Fig. 6). The various degrees of phosphate protonation is reflected in the IR and Raman spectra since the number of bands is influenced by the symmetry of the species of interest. As oxyanions adsorb on the mineral surface the symmetry is lowered, leading to peak splitting.[99] Careful considerations must be made between *in situ* analysis *vs. ex situ* analysis due to the local environment of the phosphate and Mg-surface changing with hydration/drying. A study on the calcined dolomite surface which is MgO-enriched revealed that the surface undergoes a hydration step to form –OH groups, which subsequently are converted to $-CO_3$ groups.[40] This step shows that the MgO surface does not readily adsorb phosphate, and that struvite formation requires a restructuring of the MgO surface. This surface restructuring and carbonate group formation have been observed using ATR-IR in an earlier study reporting phosphate adsorption on the $Mg(OH)_2$ surface.[100] While the use of the pseudo-second order kinetics may have been justified in the case of the MgO by assuming that the second-order is due to the phosphate species and the surface site combining, the use of pseudo-first order does not hold any physical significance since a phosphate species still combines with a surface site. However, when considering the K_{sp} values of $Mg(OH)_2$ (4.8×10^{-12})[101] and $MgCO_3$ (3.5×10^{-8})[102] it becomes evident that $MgCO_3$ is far more soluble. eqn (12) and (13) summarize the processes for surface dissolution (rate constant denotes by $k_{i,dis}$) and phosphate adsorption to form struvite (rate constant denoted by $k_{i,ads}$) for MgO and $MgCO_3$.

$$\begin{aligned} MgO + H_2O &\xrightarrow{k_{1,dis}} Mg^{2+}(\text{adsorption site}) \\ &+ PO_4^{3-} \xrightarrow{k_{1,ads}} Mg\text{–}PO_4(\text{intermediate}) \\ &+ NH_4^{+} \rightarrow \text{Struvite} \end{aligned} \quad (12)$$

$$\begin{aligned} MgCO_3 + H_2O &\xrightarrow{k_{2,dis}} Mg^{2+}(\text{adsorption site}) \\ &+ PO_4^{3-} \xrightarrow{k_{2,ads}} Mg\text{–}PO_4(\text{intermediate}) \\ &+ NH_4^{+} \rightarrow \text{Struvite} \end{aligned} \quad (13)$$

The faster surface dissolution of $MgCO_3$ (larger $k_{1,dis}$ value) allows for the faster creation of the adsorption site. This leads to faster struvite formation kinetics. In the case of MgO, the $k_{1,dis}$ value is smaller, which means that the site creation step is slower. Fig. 7 shows the –OH groups being replaced by $-CO_3$ groups before phosphate adsorption. This limits the adsorption process resulting in slower kinetics. However, as discussed above the pseudo-first order kinetics only apply when the bulk concentration change is negligible so applying this model to the $MgCO_3$ system must be reconsidered. This also raises the important questions of whether the pseudo-first order fit is a purely mathematical phenomenon that holds no physical meaning and why the pseudo-second order poorly fits the data. This may show that the expansion of the pseudo-second order model is required to accurately model some surfaces by accounting for the adsorption site formation kinetics.

A quantitative equilibrium characterization of phosphate adsorption

Quantitative equilibrium behavior analysis is typically performed using isotherms for adsorption processes. An isotherm considers the equilibrium behavior of the molecule of interest between the solid phase and the aqueous phase at a fixed temperature. Typical isotherms used for phosphate adsorption analysis are Langmuir,[27,30,36–38,43,44,73–75] Freundlich,[27,30,36–38,43,73–75] and Sips.[37] The Langmuir isotherm is one of the most widely used equations in the context of chemisorption over a wide range of conditions.[103–105] Eqn (14)

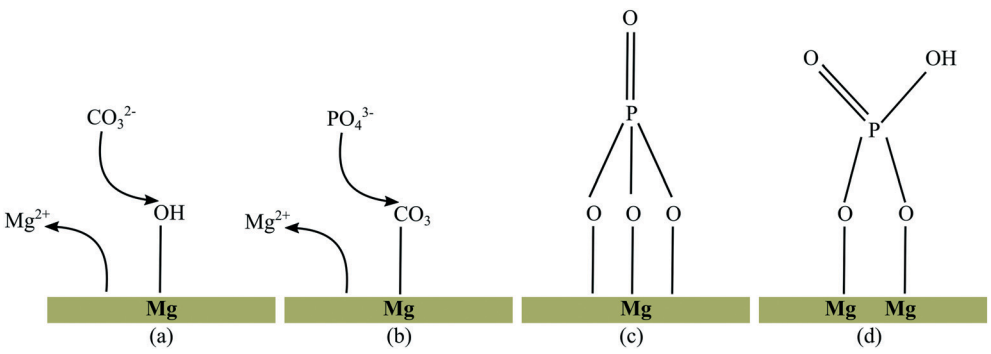

Fig. 7 (a) Carbonate group adsorption on the hydrated MgO surface (b) phosphate adsorption on the carbonate-enriched surface (c) tetrahedral phosphate adsorbed *via* inner-sphere complexation on MgO surface (d) bidentate phosphate adsorption.

shows the form of the Langmuir equation applicable to the analysis of phosphate adsorption.

$$q_e = \frac{q_m K_L C_e}{1 + K_L C_e} \quad (14)$$

Here q_m refers to a maximum adsorption capacity of phosphate, C_e denotes the equilibrium phosphate concentration in the aqueous phase, and K_L denotes the Langmuir equilibrium coefficient. The Langmuir isotherm model is based on several key assumptions: (1) adsorption occurs on a surface that is a defect-free plane, comprised of identical sites that bind one molecule per site with a monolayer denoting maximum adsorption, (2) adsorption is a reversible process, (3) the adsorption energy is identical for each molecule and is independent of molecules already adsorbed, molecules adsorbed on the surface do not interact with each other and (4) the molecules do not move laterally on the surface once they adsorb. This model, based on a homogeneous surface and ideal behavior of molecules can only be used to approximate a phosphate adsorption process since most adsorbent surfaces cannot be considered ideal, and once molecules adsorb the phosphates can interact to form chains or crystallize a solid product.[40,98,106,107] However, it is possible to derive qualitative trends or approximate equilibrium behavior using the Langmuir model. Previous work has shown that phosphate adsorption on soil can be modeled using a two-site Langmuir model.[108] This multi-site approach can lead to better fits for data on nanomaterials that have more surface area and defect sites since the adsorption sites should have varying interaction energies. Eqn (15) shows the multi-site Langmuir equation.

$$q_t = \sum_{i=1}^{n} \frac{q_{max,i} K_i C}{1 + K_i C} \quad (15)$$

Here the K_i refers to the Langmuir equilibrium constant for a species i. The Freundlich equation is shown by eqn (16) is another widely used isotherm model.[109] The Freundlich isotherm describes the active sites on a heterogeneous surface with exponential energy distribution and thus, well-fitted data suggests (but does not confirm) that the adsorbent surface is heterogeneous.

$$q_e = K_F C_e^{\frac{1}{n}} \quad (16)$$

Here the K_F denotes a Freundlich equilibrium constant while n denotes a fitting coefficient that is indicative of the binding affinity on the adsorbent surface. $n = 1$ is the special case of Henry's Law. Several Mg-based phosphate adsorbents have used Freundlich isotherms as a model along with the abovementioned Langmuir isotherm to determine the best model to describe the data but, in all cases, the Langmuir isotherm provided the best fit to the adsorption data.[27,30,36–38,43,73–75]

The Sips equation as shown by eqn (17) used by Jung *et al.* is a combination of the Langmuir and Freundlich isotherms used to analyzed MgO/biochar[75] and $MgFe_2O_4$/biochar.[37]

$$q_e = \frac{q_m K_s C_e^{\frac{1}{n}}}{1 + K_s C_e^{\frac{1}{n}}} \quad (17)$$

Using isotherms allows for the calculation of maximum adsorption capacities (from both Langmuir q_{max} and Freundlich K_F) which can help compare different adsorbent systems. Furthermore, knowing the adsorption equilibrium constant K allows for the calculation of important thermodynamic parameters such as the isosteric heat of adsorption, enthalpy of adsorption, entropy change of adsorption, and free energy change of adsorption.

The isosteric heat of adsorption ΔH_{st} is defined as the differential heat for adsorption on a fixed surface at equilibrium. This quantity has been used mostly in gas adsorption but has also been introduced in liquid-phase adsorption.[110] ΔH_{st} is calculated using the Clausius–Clapeyron eqn (18).

$$\Delta H_{st} = R \left. \frac{d \ln C_e}{d\left(\frac{1}{T}\right)} \right|_{q_e} \quad (18)$$

ΔH_{st} can be calculated by finding the C_e values using isotherms and then calculating the slope of the $\ln C_e$ *vs.* $1/T$ plot as shown in Fig. 8(a). ΔH_{st} is an important quantity in understanding the heterogeneity of the adsorbent surface. If the ΔH_{st} *vs.* q_e curve as shown in Fig. 8(b) remains constant over the range of q_e values used, the heat of adsorption does not depend on surface coverage. Therefore, the adsorption is Langmuirian in that all adsorption sites are equal in binding affinity. However, if the ΔH_{st} *vs.* q_e curve rises over the range of q_e values it becomes evident that a variety of sites with varying binding affinities exist *i.e.* the adsorption occurs on a heterogeneous surface. This type of adsorption would be associated with a process best described by the Freundlich isotherm discussed above. Therefore, examining a profile of the ΔH_{st} over experimentally derives q_e values can be beneficial in understanding the adsorption thermodynamics.

Further thermodynamic quantities that can be determined to describe the adsorption would be the change in enthalpy, change in entropy and the change in free energy. The van't

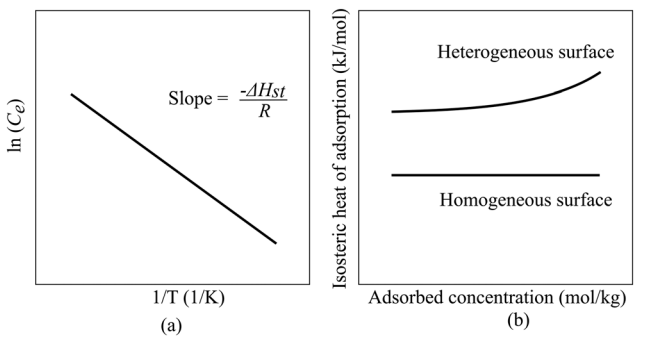

Fig. 8 (a) Example plot of $\ln C_e$ *vs.* $1/T$. (b) Example plot of ΔH_{st} *vs.* q_e for heterogeneous and homogeneous surfaces.

Hoff equation shown by eqn (19) is used to calculate the enthalpy of adsorption.

$$\Delta H^\circ = -R\frac{\mathrm{d}\ln K_c}{\mathrm{d}\left(\frac{1}{T}\right)} \quad (19)$$

K_c denotes the equilibrium constant and ΔH° denotes the change in enthalpy at a constant pressure. This K value can be derived from Langmuir and Freundlich adsorption isotherms as discussed above. The van't Hoff equation can be integrated to yield the form shown by eqn (20) which is convenient in calculating both changes in enthalpy and entropy.

$$\ln K_c = -\frac{\Delta H^\circ}{RT} + \frac{\Delta S^\circ}{R} \quad (20)$$

ΔS° denotes the change in entropy. Finally, by combining the ΔH° and ΔS° values in eqn (21) we can calculate the change in free energy (ΔG°).

$$\Delta G^\circ = \Delta H^\circ - T\Delta S^\circ \quad (21)$$

Jung *et al.* have utilized the Sips equation to calculate the K_c values, which were used to calculate the ΔH°, ΔS° and ΔG° values for phosphate adsorption on $MgFe_2O_4$.[37] They reported ΔH° as 19.501 kJ mol^{-1}, ΔS° as 0.095 kJ mol^{-1}, and ΔG° as −8.334 kJ mol^{-1}. Furthermore, they report the ΔH_{st} as a function of surface coverage and show that the surface is heterogeneous due to a rising curve. The negative free energy change shows that the adsorption is spontaneous, while the positive enthalpy change shows that the process is endothermic. Adsorption is endothermic when the adsorbent–adsorbate bond is weaker than the adsorbent–solution interactions and the adsorbate–solution phase interactions. Highly endothermic adsorption processes (ΔH° > 100 kJ mol^{-1}) indicate chemisorption *via* covalent bond formation.[85] Further heat consumption may occur due to hydrogen bonds breaking on the adsorbent surface or other surface restructuring required for adsorption. The free energy change indicates the spontaneity of the adsorption process, with spontaneous adsorption resulting in negative ΔG° values. Since the calculation of these thermodynamic parameters all depends on the equilibrium constant K, careful experimental design and execution are required to maximize the accuracy of the results.

Effects of competing cations on kinetics and product speciation

Common cations present in wastewater have been demonstrated to pose a significant impact on the kinetics of phosphate adsorption as well as product speciation due to incorporation in the product. The effects of Ca^{2+}, Cu^{2+}, Fe^{3+}, Ni^{2+}, and Zn^{2+}, Na^+, K^+, Pb^{2+}, and Cr^{3+} are among the cations that have been studied.[50,111–118] Several heavy metals that are present in wastewater pose significant health hazards to human and plant health and thus, should not be present in significant concentrations in fertilizer material produced using wastewater as the feedstock. Since US EPA and the EU have stringent restrictions on these metals incorporated in fertilizers understanding their impact on the product speciation of phosphate adsorption processes becomes important for nutrient recycling.[119,120] Since competing cations can have a severe impact on product performance (if used in nutrient recycling) and adsorption kinetics, a thorough investigation of their effects is required.

Ca^{2+} is a common cation found in many wastewater sources, ranging between 500–1500 ppm in landfill leachate and paper industry waste.[121] A previous study using $MgCO_3$ has reported the incorporation of Ca^{2+} into struvite from $CaCl_2$ and $CaCO_3$ present in the solution.[50] Ca^{2+} in high concentrations was shown to significantly inhibit struvite growth by precipitating phosphate in other phases such as hydroxyapatite as shown in other reports,[114] which is a thermodynamically favored phase due to high stability.[50] Using ATR-IR and SEM, Gray-Munro *et al.* have shown that amorphous hydroxyapatite clusters will rapidly nucleate on the $Mg(OH)_2$ surface in the presence of phosphate.[100] While this still results in phosphate removal, site blocking on the adsorbent are of concern for the process. In studies using human urine containing wastewater K^+ ions have been shown to incorporate into struvite by substituting NH_4^+ but can also have an inhibitory effect on Mg uptake in plants when incorporated into fertilizer together.[19,117,122]

A number of these studies focus on metal incorporation into struvite during phosphate capture. Some cations present in the solution phase have been found to nucleate on struvite crystals as hydroxides due to the higher pH of the experiment.[115,116] X-ray absorption spectroscopy and X-ray photoelectron spectroscopy are two key techniques used to study the oxidation state and coordination information of the metal ions incorporated into the solid phase. The presence of transition metals in wastewater during the crystallization of struvite or adsorption of phosphate using an adsorbent process operated under basic conditions can lead to heavy metal hydroxides nucleating on the phosphate product surface. This has been demonstrated on struvite recently by Tang *et al. via* an XPS study of struvite in the presence of various heavy metals.[115] Rouff *et al.* have demonstrated using EXAFS (extended X-ray absorption fine structure spectroscopy) that Zn may precipitate in the hopeite phase during struvite precipitation from $MgCl_2$ *via* homogeneous nucleation,[111] but there is a lack of studies on brucite or magnesite as the Mg source in the presence of these transition metals. Magnesite tailings[123] and dolomite[124] have been shown to adsorb Cu^{2+} and Pb^{2+} so in the presence of phosphate competitive adsorption can occur, leading to incorporation in the final product. Process design should focus on pretreatment of the wastewater to remove such contaminants if the adsorbent is expected to be recycled as a fertilizer material. Furthermore, the impact of cation precipitation on the regeneration process of the adsorbent (using an alkaline solution) should also be assessed to see if

the performance is hindered in proceeding adsorption cycles. Finally, the effect of ionic strength has not been reported for the Mg-based adsorbent systems and is an area of research that must be explored. This effect been demonstrated for phosphate adsorption on goethite, showing that in a basic environment the low ionic strength leads to lower phosphate adsorption.[125] Since phosphate recovery as struvite occurs in basic environments, the effect of ionic strength would be invaluable in tuning batch crystallization operations.

Conclusions and future research

Phosphate removal from wastewater is an important issue that should be addressed using an environmentally sustainable and economically feasible solution. Adsorption has been demonstrated to be such a feasible solution to achieve low concentrations of phosphate. Mg-Based adsorbents can be regenerated for reuse or the product of adsorption can be used as a fertilizer in the interest of nutrient recycling.[126] Potentially, inexpensive and abundant natural Mg-based minerals can also be used to tackle otherwise difficult to control phosphate emissions from non-point sources, such as agricultural fields. Mg bearing minerals such as periclase (MgO), magnesite ($MgCO_3$), dolomite ($CaMg(CO_3)_2$) occur naturally in great abundance.[16] The worldwide reserves of magnesite and brucite are estimated by the USGS to be over 12 billion tons.[16] The natural abundance of Mg bearing minerals and the well-established production and supply chain make them excellent candidates for phosphate adsorbents.

A broad variety of unsupported and supported adsorbent materials have been reported in the literature. For the design and implementation of successful phosphate adsorption and reuse process it is vital that we clearly understand kinetics, mechanism, thermodynamics, and related chemistries of phosphate adsorption under process-relevant conditions. This review summarizes the fundamentals and current state of the art for Mg-based adsorbent characterization, the kinetics of adsorption, isotherm analysis and thermodynamic parameters, adsorption mechanism, and competing ion effects. Some of the recommended future research suggestions are as follows. (1) Material characterization of adsorbents has been successful in terms of bulk characterization, but more surface-specific characterization with an emphasis on structure–performance relationships is needed to link mechanistic insights on adsorption to surface properties of adsorbents. (2) While pseudo-order models are prevalent in analyzing the kinetics of batch experiments, research interest should also move toward continuous operations and reporting kinetic parameters relevant to process design and scale-up. (3) While several studies have utilized *in situ* spectroscopic techniques to gain mechanistic insights, many reports in the literature continue to make conclusions about adsorption mechanisms using kinetics. Future research directions should focus on incorporating experimental evidence to support conclusions on mechanisms since adsorption kinetic models are often simplified and do not reflect the surface restructuring phenomena. Additionally, more studies are needed to determine whether adsorption is occurring on a surface site or whether homogeneous nucleation is occurring in a supersaturated boundary layer surrounding the adsorbent particle due to dissolution. (4) Reporting isotherms of adsorption and relevant thermodynamic parameters helps solidify the understanding of the adsorption mechanism (*i.e.* physisorption *vs.* chemisorption). Quantifying isosteric heat of adsorption, as well as enthalpy, entropy, and free energy changes of adsorption can be valuable in comparing performance as well as constructing a complete picture of the adsorption process. (5) More work is needed in understanding the effects of competing cations on the phosphate adsorption process. The cations present in wastewater can be hazardous but controlled incorporation of micronutrients allows for the production of slow-release fertilizers that can act as a new generation of fertilizers with less impact on nutrient cycles. Studying the mechanism of nucleation/adsorption as well as finding methods to pre-treat wastewater or mitigate the adsorption of these hazardous cations by controlling process conditions will be immensely important. (6) Finally, studying adsorption under realistic wastewater compositions would be of value in terms of translating the lab-scale research to pilot-scale studies. While the use of simulated wastewater helps control variables for fundamental research, applied research on studying competing ion effects and scale-up feasibility must also follow the fundamental studies of material development.

Conflicts of interest

The authors declare no conflicts of interest.

Acknowledgements

This material is based upon work supported by the National Science Foundation under Grant No. CHE 1710120.

References

1 J. N. Galloway and E. B. Cowling, Reactive Nitrogen and The World: 200 Years of Change, *Ambio*, 2002, **31**, 64–71.
2 N. Gilbert, The disappearing nutrient, *Nature*, 2009, **461**, 716–718.
3 J. Baltrusaitis, Sustainable Ammonia Production, *ACS Sustainable Chem. Eng.*, 2017, **5**, 9527–9527.
4 B. K. Mayer, L. A. Baker, T. H. Boyer, P. Drechsel, M. Gifford, M. A. Hanjra, P. Parameswaran, J. Stoltzfus, P. Westerhoff and B. E. Rittmann, Total Value of Phosphorus Recovery, *Environ. Sci. Technol.*, 2016, **50**, 6606–6620.
5 D. J. Conley, H. W. Paerl, R. W. Howarth, D. F. Boesch, S. P. Seitzinger, K. E. Havens, C. Lancelot and G. E. Likens, *Science*, 2009, **323**, 1014–1015.
6 R. J. Diaz and R. Rosenberg, Spreading Dead Zones and Consequences for Marine Ecosystems, *Science*, 2008, **321**, 926–929.

7 J. J. Beaulieu, T. DelSontro and J. A. Downing, Eutrophication will increase methane emissions from lakes and impoundments during the 21st century, *Nat. Commun.*, 2019, **10**, 1375.
8 E. Bonsdorff, K. Aarnio and E. Sandberg, Temporal and Spatial Variability of Zoobenthic Communities in Archipelago Waters of the Northern Baltic Sea-Consequences of Eutrophication?, *Int. Rev. Gesamten Hydrobiol.*, 1991, **76**, 433–449.
9 E. Bonsdorff, E. M. Blomqvist, J. Mattila and A. Norkko, Coastal eutrophication: Causes, consequences and perspectives in the archipelago areas of the Northern Baltic Sea, *Estuarine, Coastal Shelf Sci.*, 1997, **44**, 63–72.
10 D. J. Conley, J. Carstensen, G. Ærtebjerg, P. B. Christensen, T. Dalsgaard, J. L. S. Hansen and A. B. Josefson, Long-term changes and impacts of hypoxia in Danish coastal waters, *Ecol. Appl.*, 2007, **17**, S165–S184.
11 D. W. Schindler, Evolution of phosphorus limitation in lakes, *Science*, 1977, **195**, 260–262.
12 B. E. Rittmann, B. Mayer, P. Westerhoff and M. Edwards, Capturing the lost phosphorus, *Chemosphere*, 2011, **84**, 846–853.
13 J. J. Elser, Phosphorus: A limiting nutrient for humanity?, *Curr. Opin. Biotechnol.*, 2012, **23**, 833–838.
14 S. Kataki, H. West, M. Clarke and D. C. Baruah, Phosphorus recovery as struvite: Recent concerns for use of seed, alternative Mg source, nitrogen conservation and fertilizer potential, *Resour., Conserv. Recycl.*, 2016, **107**, 142–156.
15 D. Kiani, Y. Sheng, B. Lu, D. Barauskas, K. Honer, Z. Jiang and J. Baltrusaitis, Transient Struvite Formation during Stoichiometric (1:1) NH4+ and PO43– Adsorption/Reaction on Magnesium Oxide (MgO) Particles, *ACS Sustainable Chem. Eng.*, 2018, **7**, 1545–1556.
16 USGS and U.S. Geological Survey, *Mineral Commodity Summaries*, 2017.
17 B. Wu, J. Wan, Y. Zhang, B. Pan and I. M. C. Lo, Selective Phosphate Removal from Water and Wastewater using Sorption: Process Fundamentals and Removal Mechanisms, *Environ. Sci. Technol.*, 2020, **54**, 50–66.
18 M. Hauer-Jákli and M. Tränkner, Critical leaf magnesium thresholds and the impact of magnesium on plant growth and photo-oxidative defense: A systematic review and meta-analysis from 70 years of research, *Front. Plant Sci.*, 2019, **10**, 766.
19 W. Guo, S. Chen, N. Hussain, Y. Cong, Z. Liang and K. Chen, Magnesium stress signaling in plant: Just a beginning, *Plant Signaling Behav.*, 2015, **10**, e992287.
20 I. Cakmak and A. M. Yazİcİ, Magnesium: a forgotten element in crop production, *Better Crops Plant Food*, 2010, **94**, 23–25.
21 M. Tränkner, E. Tavakol and B. Jákli, Functioning of potassium and magnesium in photosynthesis, photosynthate translocation and photoprotection, *Physiol. Plant.*, 2018, **163**, 414–431.
22 W. Guo, H. Nazim, Z. Liang and D. Yang, Magnesium deficiency in plants: An urgent problem, *Crop J.*, 2016, **4**, 83–91.
23 I. Ali, New generation adsorbents for water treatment, *Chem. Rev.*, 2012, **112**, 5073–5091.
24 I. Ali, M. Asim and T. A. Khan, Low cost adsorbents for the removal of organic pollutants from wastewater, *J. Environ. Manage.*, 2012, **113**, 170–183.
25 H. Liu, X. Sun, C. Yin and C. Hu, Removal of phosphate by mesoporous ZrO2, *J. Hazard. Mater.*, 2008, **151**, 616–622.
26 P. Stolzenburg, A. Capdevielle, S. Teychené and B. Biscans, Struvite precipitation with MgO as a precursor: Application to wastewater treatment, *Chem. Eng. Sci.*, 2014, **133**, 9–15.
27 J. Zhou, S. Yang and J. Yu, Facile fabrication of mesoporous MgO microspheres and their enhanced adsorption performance for phosphate from aqueous solutions, *Colloids Surf., A*, 2011, **379**, 102–108.
28 D. A. Almasri, N. B. Saleh and M. A. Atieh, *et al.*, Adsorption of phosphate on iron oxide doped halloysite nanotubes, *Sci. Rep.*, 2019, **9**, 3232.
29 F. Liu, J. Zuo, T. Chi, P. Wang and B. Yang, Removing phosphorus from aqueous solutions by using iron-modified corn straw biochar, *Front. Environ. Sci. Eng.*, 2015, **9**, 1066–1075.
30 F. Xie, F. Wu, G. Liu, Y. Mu, C. Feng, H. Wang and J. P. Giesy, Removal of phosphate from eutrophic lakes through adsorption by in situ formation of magnesium hydroxide from diatomite, *Environ. Sci. Technol.*, 2014, **48**, 582–590.
31 J. Xie, Z. Wang, S. Lu, D. Wu, Z. Zhang and H. Kong, Removal and recovery of phosphate from water by lanthanum hydroxide materials, *Chem. Eng. J.*, 2014, **254**, 163–170.
32 D. Wu, B. Zhang, C. Li, Z. Zhang and H. Kong, Simultaneous removal of ammonium and phosphate by zeolite synthesized from fly ash as influenced by salt treatment, *J. Colloid Interface Sci.*, 2006, **304**, 300–306.
33 J. Xie, Z. Wang, D. Fang, C. Li and D. Wu, Green synthesis of a novel hybrid sorbent of zeolite/lanthanum hydroxide and its application in the removal and recovery of phosphate from water, *J. Colloid Interface Sci.*, 2014, **423**, 13–19.
34 H. Bacelo, A. M. A. Pintor, S. C. R. Santos, R. A. R. Boaventura and C. M. S. Botelho, Performance and prospects of different adsorbents for phosphorus uptake and recovery from water, *Chem. Eng. J.*, 2020, **381**, 122566.
35 P. S. Kumar, L. Korving, M. C. M. van Loosdrecht and G. J. Witkamp, Adsorption as a technology to achieve ultra-low concentrations of phosphate: Research gaps and economic analysis, *Water Res. X*, 2019, **4**, 100029.
36 R. Li, J. J. Wang, Z. Zhang, M. K. Awasthi, D. Du, P. Dang, Q. Huang, Y. Zhang and L. Wang, Recovery of phosphate and dissolved organic matter from aqueous solution using a novel CaO-MgO hybrid carbon composite and its feasibility in phosphorus recycling, *Sci. Total Environ.*, 2018, **642**, 526–536.
37 K. W. Jung, S. Lee and Y. J. Lee, Synthesis of novel magnesium ferrite (MgFe2O4)/biochar magnetic composites and its adsorption behavior for phosphate in aqueous solutions, *Bioresour. Technol.*, 2017, **245**, 751–759.

38 R. Li, J. J. Wang, B. Zhou, M. K. Awasthi, A. Ali, Z. Zhang, A. H. Lahori and A. Mahar, Recovery of phosphate from aqueous solution by magnesium oxide decorated magnetic biochar and its potential as phosphate-based fertilizer substitute, *Bioresour. Technol.*, 2016, **215**, 209–214.

39 P. Xia, X. Wang, X. Wang, J. Song, H. Wang and J. Zhang, Struvite crystallization combined adsorption of phosphate and ammonium from aqueous solutions by mesoporous MgO–loaded diatomite, *Colloids Surf., A*, 2016, **506**, 220–227.

40 D. Kiani, M. Silva, Y. Sheng and J. Baltrusaitis, Experimental Insights into the Genesis and Growth of Struvite Particles on Low-Solubility Dolomite Mineral Surfaces, *J. Phys. Chem. C*, 2019, **123**, 25135–25145.

41 J. M. Vanson, A. Boutin, M. Klotz and F. X. Coudert, Transport and adsorption under liquid flow: the role of pore geometry, *Soft Matter*, 2017, **13**, 875–885.

42 J. R. H. Ross, in *Contemporary Catalysis*, Elsevier, 2019, pp. 39–68.

43 J. Lin, S. He, X. Wang, H. Zhang and Y. Zhan, Removal of phosphate from aqueous solution by a novel Mg(OH)2/ZrO2 composite: Adsorption behavior and mechanism, *Colloids Surf., A*, 2019, **561**, 301–314.

44 M. Zhang, B. Gao, Y. Yao, Y. Xue and M. Inyang, Synthesis of porous MgO-biochar nanocomposites for removal of phosphate and nitrate from aqueous solutions, *Chem. Eng. J.*, 2012, **210**, 26–32.

45 F. Demir, O. Laçin and B. Dönmez, Leaching kinetics of calcined magnesite in citric acid solutions, *Ind. Eng. Chem. Res.*, 2006, **45**, 1307–1311.

46 S. Ahmed and A. Iqbal, Synthesis of 2D Magnesium Oxide Nanosheets: A Potential Material for Phosphate Removal, *Glob. Chall.*, 2018, **2**, 1800056.

47 J. Li, X. Wang, J. Wang, Y. Li, S. Xia and J. Zhao, Simultaneous recovery of microalgae, ammonium and phosphate from simulated wastewater by MgO modified diatomite, *Chem. Eng. J.*, 2019, **362**, 802–811.

48 J. Lin, S. He, Y. Zhan and H. Zhang, Evaluation of phosphate adsorption on zirconium/magnesium-modified bentonite, *Environ. Technol.*, 2020, **41**, 586–602.

49 H. P. Jing, Y. Li, X. Wang, J. Zhao and S. Xia, Simultaneous recovery of phosphate, ammonium and humic acid from wastewater using a biochar supported Mg(OH)2/bentonite composite, *Environ. Sci.: Water Res. Technol.*, 2019, **5**, 931–943.

50 B. Lu, D. Kiani, W. Taifan, D. Barauskas, K. Honer, L. Zhang and J. Baltrusaitis, Spatially Resolved Product Speciation during Struvite Synthesis from Magnesite (MgCO 3) Particles in Ammonium (NH 4 +) and Phosphate (PO 4 3−) Aqueous Solutions, *J. Phys. Chem. C*, 2019, **123**(14), 8908–8922.

51 J. Chen, L. G. Yan, H. Q. Yu, S. Li, L. L. Qin, G. Q. Liu, Y. F. Li and B. Du, Efficient removal of phosphate by facile prepared magnetic diatomite and illite clay from aqueous solution, *Chem. Eng. J.*, 2016, **287**, 162–172.

52 M. Quintana, E. Sánchez, M. F. Colmenarejo, J. Barrera, G. García and R. Borja, Kinetics of phosphorus removal and struvite formation by the utilization of by-product of magnesium oxide production, *Chem. Eng. J.*, 2005, **111**, 45–52.

53 M. Quintana, M. F. Colmenarejo, J. Barrera, G. García, E. García and A. Bustos, Use of a Byproduct of Magnesium Oxide Production To Precipitate Phosphorus and Nitrogen as Struvite from Wastewater Treatment Liquors, *J. Agric. Food Chem.*, 2004, **52**, 294–299.

54 B. D. Cullity and S. R. Stock, *Elements of X-ray Diffraction*, Prentice-Hall, 3rd edn, 2001.

55 J. Goldstein, D. E. Newbury, D. C. Joy, C. E. Lyman, P. Echlin, E. Lifshin, L. Sawyer and J. R. Michael, *Scanning Electron Microscopy and X-ray Microanalysis*, ed. J. Goldstein, Springer US, 2003.

56 S. Nasrazadani and S. Hassani, in *Handbook of Materials Failure Analysis with Case Studies from the Oil and Gas Industry*, Elsevier Inc., 2016, pp. 39–54.

57 N. Khare, D. Hesterberg and J. D. Martin, XANES investigation of phosphate sorption in single and binary systems of iron and aluminum oxide minerals, *Environ. Sci. Technol.*, 2005, **39**, 2152–2160.

58 W. Li, X. Feng, Y. Yan, D. L. Sparks and B. L. Phillips, Solid-state NMR spectroscopic study of phosphate sorption mechanisms on aluminum (hydr)oxides, *Environ. Sci. Technol.*, 2013, **47**, 8308–8315.

59 J. Kim, W. Li, B. L. Philips and C. P. Grey, Phosphate adsorption on the iron oxyhydroxides goethite (α-FeOOH), akaganeite (β-FeOOH), and lepidocrocite (γ-FeOOH): A 31P NMR Study, *Energy Environ. Sci.*, 2011, **4**, 4298–4305.

60 S. Brunauer, P. H. Emmett and E. Teller, Adsorption of Gases in Multimolecular Layers, *J. Am. Chem. Soc.*, 1938, **60**, 309–319.

61 E. P. Barrett, L. G. Joyner and P. P. Halenda, The Determination of Pore Volume and Area Distributions in Porous Substances. I. Computations from Nitrogen Isotherms, *J. Am. Chem. Soc.*, 1951, **73**, 373–380.

62 D. Zhu, Y. Chen, H. Yang, S. Wang, X. Wang, S. Zhang and H. Chen, Synthesis and characterization of magnesium oxide nanoparticle-containing biochar composites for efficient phosphorus removal from aqueous solution, *Chemosphere*, 2020, **247**, 125847.

63 C. V. Cushman, P. Brüner, J. Zakel, G. H. Major, B. M. Lunt, N. J. Smith, T. Grehl and M. R. Linford, *Anal. Methods*, 2016, **8**, 3419–3439.

64 H. H. Brongersma, M. Draxler, M. de Ridder and P. Bauer, Surface composition analysis by low-energy ion scattering, *Surf. Sci. Rep.*, 2007, **62**, 63–109.

65 J. Druce, H. Téllez, M. Burriel, M. D. Sharp, L. J. Fawcett, S. N. Cook, D. S. McPhail, T. Ishihara, H. H. Brongersma and J. A. Kilner, Surface termination and subsurface restructuring of perovskite-based solid oxide electrode materials, *Energy Environ. Sci.*, 2014, **7**, 3593–3599.

66 H. N. Tran, S. J. You, A. Hosseini-Bandegharaei and H. P. Chao, Mistakes and inconsistencies regarding adsorption of contaminants from aqueous solutions: A critical review, *Water Res.*, 2017, **120**, 88–116.

67 M. A. Bañares and I. E. Wachs, in *Encyclopedia of Analytical Chemistry*, John Wiley & Sons, Ltd, Chichester, UK, 2010.
68 N. Kumar, C. S. Wondergem, A. J. Wain and B. M. Weckhuysen, In Situ Nanoscale Investigation of Catalytic Reactions in the Liquid Phase Using Zirconia-Protected Tip-Enhanced Raman Spectroscopy Probes, *J. Phys. Chem. Lett.*, 2019, **10**, 1669–1675.
69 A. G. Young and A. J. McQuillan, Adsorption/desorption kinetics from ATR-IR spectroscopy. Aqueous oxalic acid on anatase TiO2, *Langmuir*, 2009, **25**, 3538–3548.
70 S. J. Hug and B. Sulzberger, In Situ Fourier Transform Infrared Spectroscopic Evidence for the Formation of Several Different Surface Complexes of Oxalate on TiO2 in the Aqueous Phase, *Langmuir*, 1994, **10**, 3587–3597.
71 E. J. Elzinga and D. L. Sparks, Phosphate adsorption onto hematite: An in situ ATR-FTIR investigation of the effects of pH and loading level on the mode of phosphate surface complexation, *J. Colloid Interface Sci.*, 2007, **308**, 53–70.
72 B. Wang, X. Xiong, H. Ren and Z. Huang, Preparation of MgO nanocrystals and catalytic mechanism on phenol ozonation, *RSC Adv.*, 2017, **7**, 43464–43473.
73 M. El Bouraie and A. A. Masoud, Adsorption of phosphate ions from aqueous solution by modified bentonite with magnesium hydroxide Mg(OH)2, *Appl. Clay Sci.*, 2017, **140**, 157–164.
74 R. Li, J. J. Wang, B. Zhou, M. K. Awasthi, A. Ali, Z. Zhang, L. A. Gaston, A. H. Lahori and A. Mahar, Enhancing phosphate adsorption by Mg/Al layered double hydroxide functionalized biochar with different Mg/Al ratios, *Sci. Total Environ.*, 2016, **559**, 121–129.
75 K. W. Jung and K. H. Ahn, Fabrication of porosity-enhanced MgO/biochar for removal of phosphate from aqueous solution: Application of a novel combined electrochemical modification method, *Bioresour. Technol.*, 2016, **200**, 1029–1032.
76 S. Lagergren, About the Theory of So-Called Adsorption of Soluble Substances, *K. Sven. Vetenskapsakad. Handl.*, 1898, **24**, 1–39.
77 Y. S. Ho and G. McKay, A Comparison of chemisorption kinetic models applied to pollutant removal on various sorbents, *Process Saf. Environ. Prot.*, 1998, **76**, 332–340.
78 S. Azizian, Kinetic models of sorption: A theoretical analysis, *J. Colloid Interface Sci.*, 2004, **276**, 47–52.
79 W. Rudzinski and W. Plazinski, Kinetics of solute adsorption at solid/solution interfaces: A theoretical development of the empirical pseudo-first and pseudo-second order kinetic rate equations, based on applying the statistical rate theory of interfacial transport, *J. Phys. Chem. B*, 2006, **110**, 16514–16525.
80 W. Rudzinski and W. Plazinski, Studies of the kinetics of solute adsorption at solid/solution interfaces: On the possibility of distinguishing between the diffusional and the surface reaction kinetic models by studying the pseudo-first-order kinetics, *J. Phys. Chem. C*, 2007, **111**, 15100–15110.
81 G. McKay, Y. S. Ho and J. C. Y. Ng, Biosorption of copper from waste waters: A review, *Sep. Purif. Methods*, 1999, **28**, 87–125.
82 G. Blanchard, M. Maunaye and G. Martin, Removal of heavy metals from waters by means of natural zeolites, *Water Res.*, 1984, **18**, 1501–1507.
83 K. L. Tan and B. H. Hameed, Insight into the adsorption kinetics models for the removal of contaminants from aqueous solutions, *J. Taiwan Inst. Chem. Eng.*, 2017, **74**, 25–48.
84 S. P. D. Monte Blanco, F. B. Scheufele, A. N. Módenes, F. R. Espinoza-Quiñones, P. Marin, A. D. Kroumov and C. E. Borba, Kinetic, equilibrium and thermodynamic phenomenological modeling of reactive dye adsorption onto polymeric adsorbent, *Chem. Eng. J.*, 2017, **307**, 466–475.
85 Y. Tong, P. J. McNamara and B. K. Mayer, *Environ. Sci.: Water Res. Technol.*, 2019, **5**, 821–838.
86 Y. S. Ho, J. C. Y. Ng and G. McKay, Kinetics of pollutant sorption by biosorbents: Review, *Sep. Purif. Methods*, 2000, **29**, 189–232.
87 C. Aharoni and F. C. Tompkins, Kinetics of Adsorption and Desorption and the Elovich Equation, *Adv. Catal.*, 1970, **21**, 1–49.
88 G. Parravano and M. Boudart, Chemisorption and Catalysis on Oxide Semiconductors, *Adv. Catal.*, 1955, **7**, 47–74.
89 R. S. Juang and M. L. Chen, Application of the Elovich Equation to the Kinetics of Metal Sorption with Solvent-Impregnated Resins, *Ind. Eng. Chem. Res.*, 1997, **36**, 813–820.
90 *Wastewater Report 2018: The reuse opportunity*, World, ReliefWeb, Vienna, 2018.
91 C. Tien, *Adsorption Calculations and Modelling*, Butterworth-Heinemann, 1994.
92 W. J. Weber and J. C. Morris, Kinetics of Adsorption on Carbon from Solution, *J. Sanit. Eng. Div., Am. Soc. Civ. Eng.*, 1963, **89**, 31–60.
93 Z. Zha, Y. Ren, S. Wang, Z. Qian, L. Yang, P. Cheng, Y. Han and M. Wang, Phosphate adsorption onto thermally dehydrated aluminate cement granules, *RSC Adv.*, 2018, **8**, 19326–19334.
94 L. Hou, Q. Liang and F. Wang, Mechanisms that control the adsorption-desorption behavior of phosphate on magnetite nanoparticles: The role of particle size and surface chemistry characteristics, *RSC Adv.*, 2020, **10**, 2378–2388.
95 O. Fruhwirth, G. W. Herzog, I. Hollerer and A. Rachetti, Dissolution and hydration kinetics of MgO, *Surf. Technol.*, 1985, **24**, 301–317.
96 A. Putnis and C. V. Putnis, The mechanism of reequilibration of solids in the presence of a fluid phase, *J. Solid State Chem.*, 2007, **180**, 1783–1786.
97 E. Ruiz-Agudo, C. V. Putnis and A. Putnis, Coupled dissolution and precipitation at mineral-fluid interfaces, *Chem. Geol.*, 2014, **383**, 132–146.
98 J. Hövelmann and C. V. Putnis, In Situ nanoscale imaging of struvite formation during the dissolution of natural brucite: Implications for phosphorus recovery from wastewaters, *Environ. Sci. Technol.*, 2016, **50**, 13032–13041.
99 G. Lefèvre, In situ Fourier-transform infrared spectroscopy studies of inorganic ions adsorption on metal oxides and hydroxides, *Adv. Colloid Interface Sci.*, 2004, **107**, 109–123.

100 J. E. Gray-Munro and M. Strong, A study on the interfacial chemistry of magnesium hydroxide surfaces in aqueous phosphate solutions: Influence of Ca2+, Cl- and protein, *J. Colloid Interface Sci.*, 2013, **393**, 421–428.
101 A. A. Al-Hamzah, E. J. Smith and C. M. Fellows, Inhibition of homogeneous formation of magnesium hydroxide by low-molar-mass poly(acrylic acid) with different end-groups, *Ind. Eng. Chem. Res.*, 2015, **54**, 2201–2207.
102 Z.-Y. Chen, W. K. O'Connor and S. J. Gerdemann, Chemistry of aqueous mineral carbonation for carbon sequestration and explanation of experimental results, *Environ. Prog.*, 2006, **25**, 161–166.
103 I. Langmuir, The adsorption of gases on plane surfaces of glass, mica and platinum, *J. Am. Chem. Soc.*, 1918, **40**, 1361–1403.
104 I. Langmuir, The constitution and fundamental properties of solids and liquids. Part I. Solids, *J. Am. Chem. Soc.*, 1916, **38**, 2221–2295.
105 I. Langmuir, The constitution and fundamental properties of solids and liquids. II. Liquids, *J. Am. Chem. Soc.*, 1917, **39**, 1848–1906.
106 S. Lee, H. S. Wi, W. Jo, Y. C. Cho, H. H. Lee, S.-Y. Jeong, Y.-I. Kim and G. W. Lee, Multiple pathways of crystal nucleation in an extremely supersaturated aqueous potassium dihydrogen phosphate (KDP) solution droplet, *Proc. Natl. Acad. Sci. U. S. A.*, 2016, **113**, 13618–13623.
107 K. A. Syed, S. F. Pang, Y. Zhang, G. Zeng and Y. H. Zhang, Micro-Raman observation on the HPO42- association structures in an individual dipotassium hydrogen phosphate (K2HPO 4) droplet, *J. Phys. Chem. A*, 2012, **116**, 1558–1564.
108 I. C. R. Holford, R. W. M. Wedderburn and G. E. G. Mattingly, A Langmuir two-surface equation as a model for phosphate adsorption by soils, *J. Soil Sci.*, 1974, **25**, 242–255.
109 H. Freundlich, Of the adsorption of gases. Section II. Kinetics and energetics of gas adsorption. Introductory paper to section II, *Trans. Faraday Soc.*, 1932, **28**, 195–201.
110 S. Builes, S. I. Sandler and R. Xiong, Isosteric heats of gas and liquid adsorption, *Langmuir*, 2013, **29**, 10416–10422.
111 A. A. Rouff and K. M. Juarez, Zinc Interaction with Struvite During and After Mineral Formation, *Environ. Sci. Technol.*, 2014, **48**, 6342–6349.
112 A. A. Rouff, M. V. Ramlogan and A. Rabinovich, Synergistic Removal of Zinc and Copper in Greenhouse Waste Effluent by Struvite, *ACS Sustainable Chem. Eng.*, 2016, **4**, 1319–1327.
113 M. Ronteltap, M. Maurer and W. Gujer, The behaviour of pharmaceuticals and heavy metals during struvite precipitation in urine, *Water Res.*, 2007, **41**, 1859–1868.
114 K. S. Le Corre, E. Valsami-Jones, P. Hobbs and S. A. Parsons, Impact of calcium on struvite crystal size, shape and purity, *J. Cryst. Growth*, 2005, **283**, 514–522.
115 C. Tang, Z. Liu, C. Peng, L. Y. Chai, K. Kuroda, M. Okido and Y. X. Song, New insights into the interaction between heavy metals and struvite: Struvite as platform for heterogeneous nucleation of heavy metal hydroxide, *Chem. Eng. J.*, 2019, **365**, 60–69.
116 H. Arslanoglu, Adsorption of micronutrient metal ion onto struvite to prepare slow release multielement fertilizer: Copper(II) doped-struvite, *Chemosphere*, 2019, **217**, 393–401.
117 H. Huang, D. Zhang, W. Wang, B. Li, N. Zhao, J. Li and J. Dai, Alleviating Na+ effect on phosphate and potassium recovery from synthetic urine by K-struvite crystallization using different magnesium sources, *Sci. Total Environ.*, 2019, **655**, 211–219.
118 A. A. Rouff, Sorption of chromium with struvite during phosphorus recovery, *Environ. Sci. Technol.*, 2012, **46**, 12493–12501.
119 O. US EPA, Agriculture Nutrient Management and Fertilizer.
120 V. Halleux, *EU fertilising products*, 2019.
121 F. Hammes, A. Seka, S. De Knijf and W. Verstraete, A novel approach to calcium removal from calcium-rich industrial wastewater, *Water Res.*, 2003, **37**, 699–704.
122 I. Cakmak, Magnesium in crop production, food quality and human health, *Plant Soil*, 2013, **368**, 1–4.
123 İ. Kıpçak and T. G. Isıyel, Magnesite tailing as low-cost adsorbent for the removal of copper (II) ions from aqueous solution, *Korean J. Chem. Eng.*, 2015, **32**, 1634–1641.
124 E. Pehlivan, A. M. Özkan, S. Dinç and Ş. Parlayici, Adsorption of Cu2+ and Pb2+ ion on dolomite powder, *J. Hazard. Mater.*, 2009, **167**, 1044–1049.
125 J. Antelo, M. Avena, S. Fiol, R. López and F. Arce, Effects of pH and ionic strength on the adsorption of phosphate and arsenate at the goethite-water interface, *J. Colloid Interface Sci.*, 2005, **285**, 476–486.
126 A. Drenkova-Tuhtan, M. Schneider, K. Mandel, C. Meyer, C. Gellermann, G. Sextl and H. Steinmetz, Influence of cation building blocks of metal hydroxide precipitates on their adsorption and desorption capacity for phosphate in wastewater-A screening study, *Colloids Surf., A*, 2016, **488**, 145–153.
127 M. Silva, V. Murzin, L. Zhang, J. Baltrus and J. Baltrusaitis, Transition metal-doped MgO nanoparticles for nutrient recycling: an alternate Mg source for struvite synthesis from wastewater, *Environ. Sci.: Nano*, 2020, DOI: 10.1039/D0EN00660B.